THESIS FOR THE DEGREE OF LICENTIATE OF ENGINEERING

From Eulerian to Lagrangian Viewpoints in Fluid Flows

Convective Chaotic Mixing in Microfluidics

Erik Svensson

CHALMERS | GÖTEBORG UNIVERSITY

Department of Computational Mathematics
Chalmers University of Technology and Göteborg University
Göteborg, Sweden 2003

This work was supported by:
The Network in Applied Mathematics;
The Swedish Foundation for Strategic Research; and
IMEGO, the Institute of Microelectronics in Gothenburg

From Eulerian to Lagrangian Viewpoints in Fluid Flows: Convective Chaotic Mixing in Microfluidics
Erik Svensson
ISSN 0347-2809/NO. 2003:62

Department of Computational Mathematics
Chalmers University of Technology and Göteborg University
SE-412 96 Göteborg
Sweden
Telephone +46 (0)31 772 1000

Cover: A flow trajectory in the dense herringbone mixer projected onto the yz-plane, and the deformation of a circle along the trajectory.

Printed in Göteborg, Sweden 2003

From Eulerian to Lagrangian Viewpoints in Fluid Flows

Convective Chaotic Mixing in Microfluidics

Erik Svensson

Department of Computational Mathematics
Chalmers University of Technology
Göteborg University

Abstract

Fluid mixing in small systems is difficult when the diffusion is a slow process compared to other relevant processes, and when the fluid dynamics is laminar, *i.e.*, dominated by viscous forces. This is the prevailing situation in microfluidic systems. However, mixing is enhanced in chaotic flows. In this work we estimate and compute the mixing time in chaotic channel flows as $t_m = 1/(2\sigma)\ln(\mathrm{Pe})$, where σ is related to a stability factor for the flow and Pe is the Péclet number.

We compute the flow in a number of realistic microfluidic mixers by solving the stationary three-dimensional Navier-Stokes equations and Stokes equations by the finite element method. Stability factors are obtained by computing and analyzing flow trajectories. The procedure is motivated by maximum norm *a priori* error estimates quoted from the literature.

A major part of this work has been to choose, evaluate, and implement algorithms. The implemented Navier-Stokes/Stokes solver, written in C++ code, combines a Krylov method with multigrid. Our results indicate that the solver is optimal.

Keywords: mixing, chaotic convection, microfluidics, microfluids, Navier-Stokes, Lagrangian viewpoint, preconditioner, multigrid, Hood-Taylor, finite element

Preface

This thesis is submitted in partial fulfilment of the requirements for: a licentiate degree in computational mathematics at Chalmers University of Technology, and the post-graduate program in industrial mathematics organized by ECMI, European Consortium for Mathematics in Industry.

The licentiate degree, customary to many Swedish Universities, is an intermediate degree that Ph.D. candidates are encouraged to fulfill. The notion is unfamiliar in most other countries, and hence, it is difficult to relate. However, the licentiate degree is acknowledged as a degree in Sweden, but for many Ph.D. candidates the licentiate thesis is merely a 'midterm report'.

The ECMI post-graduate program is designed to improve the participants interdisciplinary skills; and to promote and nourish the use of mathematical methods in industry. The present work has been in close collaboration with the industrial partner IMEGO, the Institute of Microelectronics in Gothenburg.

Göteborg, December 2003
Erik Svensson

Contents

1. Introduction

One of the major themes in technology and science during the past half century has been miniaturization. As a most notable consequence the performance of computers is improving at an exponential rate. The number of transistors per area unit in an integrated circuit is doubled every 1.5 year. This is known as Moore's law in honor of Gordon Moore who made this prediction nearly forty years ago [50]. This is likely to go on for 10–15 more years and then start to level out when the size of the transistor is approaching the molecular size [4]. From an engineering/computational point of view this is promising[1]. We may expect that computer simulations will become even more important both in fundamental research and industrial design. The traditional experiments will to some extent be replaced by 'virtual experiments', gaining efficiency, flexibility and cutting costs. This is not only academic chit-chat. The market for prototyping software is estimated [20] to 1.4 billion dollars year 2007.
Miniaturization does not only encompass electronics and impact on computer technology. New fields are emerging where electronics is merged with mechanics, in *micro-electro-mechanical systems* (MEMS) and fluid systems are scaled down in size, in *microfluidics*. The present work will mainly deal with computational aspects of large scale computing related to microfluidics and with particular applications to fluid mixing in microchannels.

1.1. **Microfluidics.**

What is microfluidics? It is difficult to give a terse definition and it is probably meaningless to try anyway. We have a notion of microelectronics. Thus, let us say that microfluidics is like microelectronics but instead of charge transport as for microelectronics, microfluidics is mainly about atom and molecular mass transport in microsystems. Microelectronics could be combined with micromechanics and microfluidics in MEMS devices. This possibility is of utmost practical importance since the combination naturally enlarges the functionality and the number of devices that could be produced and studied, possible also opens up for new applications.

We make a distinction between *microfluidic* and *microfluid* systems and say that the microfluidic systems are manmade systems whereas microfluid systems is a collective name for all small fluid systems. Microfluidic systems are fabricated with similar techniques as is used for microelectronics,

[1] But also daunting since today there is no successor to the silicon technology.

e.g., lithography *etc.*, and could for this reason in a natural way be included in MEMS devices. Microfluid systems in general could for example be found in nature, *e.g.*, thin blood vessels and cells. Another important example related to microfluid systems is the microscale flow between particles in colloidal dispersions. This intricate flow governs the hydrodynamical interaction in colloidal systems.

From an applied mathematical perspective microfluidic and MEMS technology include a lot of physics that could be appropriately modelled with partial differential equations, e.g., the *convection-diffusion-reaction* equation for heat and chemical reactants, the *Maxwell* equations for the electromagnetic field, the *Navier-Stokes* equations for fluid transport and the *elasticity* equation for solid mechanics, *etc.* It is a strong mathematical result that there exist unique solutions to the mentioned equations[2]. With a powerful computer at hand and with multi-physics models (combining the equations above) it should be possible to describe, design and to a large extent understand microfluidic and MEMS devices through computer simulations.

For general reference on microfluidics we refer to the monograph [41] and a number of review and research articles [74, 10, 26, 47].

1.1.1. *Science.* In microfluidics, as we scale down the size of the system, it becomes more important to understand various types of interactions in the flow and the underlying physical mechanisms. These interactions are: **(*i*)** the interaction between the constituents of the flow, molecules and particles, for example, the hydrodynamical interaction between particles in colloidal dispersions; and **(*ii*)** the interaction between solid objects, such as walls, and the fluid. These interactions are not fully understood and are subjects to fundamental research. By exploring microfluidic devices we may gain in fundamental understanding of how matter interacts, knowledge useful if we for example would like to understand friction and lubrication.

Remark 1.1. Through this work we will frequently use two dimensionless numbers:
(*i*) The *Reynolds number*, Re, estimating the ratio of inertia to viscous forces in a flow, $\mathrm{Re} = UL/\mu$, where L and U are characteristic length and

[2]With exception to the Navier-Stokes equations where the issue is an open question worth a million dollars [64]. However we may expect the existence of a unique solution for laminar flows, close to Stokes flow.

velocity scales of the system, $\mu = \eta/\rho$ is the kinematic viscosity, η is the fluid viscosity and ρ is the fluid density ($\mu = 10^{-6}\,[m^2/s]$ for water).
(ii) The *Péclet number*, Pe, estimating the ratio of convective to diffusive processes in the flow, $\mathrm{Pe} = LU/D$, where D is the diffusion coefficient.

We summarize a few features associated with microfluidics.
Small Reynolds number, $\mathrm{Re} \lesssim$ **10.** Fluid flows in microstructures are usually limited by the size of the system, friction to walls, and therefore the fluid velocity will be small. Combining this with the size of the system generally gives a Reynolds number $\mathrm{Re} \lesssim 10$ or possibly $Re \ll 10$. Inertia will play a minor role in microfluidics and there will not be any turbulence in a traditional meaning, although elastic turbulence may occur [29, 30] but this is due to an entirely different mechanism.
Large Péclet number, $\mathrm{Pe} \gtrsim$ **100.** The diffusion of particles/(molecules) is approximately inversely proportional to the size of the particle. For dilute solutions the diffusion coefficient of a particle could be estimated by a Brownian motion type of argument to $D = k_B T/(6\pi\eta a)$ where k_B is the Boltzmann constant, T is the temperature, η is the viscosity of the fluid and a is the size of the particle [16]. The diffusion coefficient is small for large molecules, such as, DNA, proteins, cells, or generally, for colloidal particles and therefore the Péclet number will be large for many microfluid systems of interest, approximately $\mathrm{Pe} \gtrsim 100$. As a consequence fluid mixing is difficult in microfluidic systems.
Slip boundary condition. The *non-slip* boundary condition, *i.e.*, that the fluid takes the same velocity as the solid at the solid-fluid interface, is often taken for granted in macroscopic models, for an exception see [65]. In microfluidics we should hesitate before applying a non-slip boundary condition. There is a large number of studies pointing in the direction that there is *slip* at the solid fluid interface, see for example [75, 14, 12]. To get a feel for how a slip boundary condition may influence the flow field we solve the Navier-Stokes equations in the domain between the planes $y = \pm h$ and with a constant pressure gradient Δp in the x-direction. Assuming a linear Navier boundary condition [65], that is, $u(y = \pm h) = \beta\dot{\gamma}$ where β is the slip length and $\dot{\gamma}$ is the shear rate[3], we get,

$$u = \frac{h^2 \Delta p}{2\eta}\left(\left(\frac{y}{h}\right)^2 - 1 - \frac{2\beta}{h}\right). \tag{1.1}$$

[3] $\dot{\gamma} = n \cdot \nabla u$, where n is the unit normal pointing into the domain.

The slip length, β, is generally in the micrometer regime and hence the influence from the slip becomes larger as the size of the system is scaled down. This should be compared to the solution in the non-slip case, $u = (h^2\Delta p/2\eta)((y/h)^2 - 1)$.

Granularity and failure of the continuum hypothesis. The continuum hypothesis for fluid mechanics is valid when the fluid system length and time scales are considerably larger than the largest molecular length and time scales, the fluid system should always be in local thermodynamical equilibrium. In microfluidics we carefully have to consider the validity of the continuum hypothesis. In reality there is no such thing as a continuum, the constituents in flows are atoms or molecules. As we scale down the size of a fluid system this becomes more and more apparent. When the continuum hypothesis is violated one must reconsider the model used for describing the flow, if it is a continuum model. For gas flows this happens when the mean free path of the gas molecules approach the size of the fluid system. This is captured by the Knudsen number and we refer to [47, 15] for further details. For fluids this type of effect is more subtle. There may be reorientation of the molecular structure of the fluid in a thin layer at, for example, solid-fluid interfaces [41] and fluctuations due to molecular diffusion on the solid-fluid interface [51]. There is yet another effect related to dilution, consider for example a fluid containing dissolved/dispersed particles/molecules. For small systems it might not be correct to introduce the notion of concentration for particles or molecules, due to fluctuations that may arise in this continuum variable. This is similar to rarefication in gas flows. For particle flows it may even be necessary to include the particles in a direct numerical simulation in order to accurately describe the system. This should be necessary when the size of the particles approach a large fraction of the size of the system.

1.1.2. *Technology.* The size of beakers, test tubes, tubings *etc.* in a chemistry laboratory has been more or less constant over the past 300 years [62]. Microfluidics will drastically change this and revolutionize chemistry in a similar way as microelectronics revolutionized electronics. Microfluidics will set a new paradigm for chemical analysis, reducing solvent and sample consumption, and in this way gain efficiency, cutting time and costs [32]. Microfluidics will also make it possible to design and control chemical experiments, reactions and processes on the microscopic scale. This opens up the possibility to better improve reaction rate constants and also to

have a better control on by-products, that could for example be toxic and harmful for the environment [33].

Today entire fluid systems, channels, sample reservoirs, pumps and valves are scaled down and integrated onto microchips [66]. When combining this infrastructure with analysis devices it is common practice to talk about 'lab on a chip' [59]. The step taken, integrating the fluid system on a chip is gigantic in terms of the possibility to increase complexity and to make it possible for automated (computerized) control. The allegory *tyranny of numbers*, historically known from computer design[4], could be recast into *tyranny of pipetteing* for a modern chemistry laboratory [66].

It was early recognized that microchannels could possibly be used for cooling of microelectronic circuits [55]. Today we see a number of other applications related to biotechnology such as DNA and protein analysis [11], particle separation and detection [72], fluid control [31], but also generally for chemical reactions and synthesis [22].

1.2. **Aim.** It is intrinsically difficult to mix fluids in microfluidic systems, see for example [61, 43]. Work done in the direction of understanding and improving mixing in microfluidic systems found in the literature are mainly experimental [61, 46, 63]. The overall aim of the present work is to:

1. Establish a quantitative criterion that will describe the mixing properties (good/bad) in microfluidic systems.
2. Simulate the dynamics of fluid flow in microfluidic systems.

1.3. **Motivation.**

1.3.1. *Computational mathematics.* The tremendous development of computer power that we have experienced during the past three decades and that probably will continue for at least one more decade must be accompanied with development of computational methods. We would like to solve *partial differential equations* (PDEs) in realistic settings, which often means that we will have to work with three spatial dimensions. Unavoidably the degrees of freedom and hence the size of the problems will become large in three dimensions. A draw-back of many commercially available

[4]It became impractical at the time to build computers out of vacuum tubes because the number of vacuum tubes became too large with the consequence that the computer became to 'bulky' and there was a real problem in wiring the components together. The tyranny of numbers was resolved by the dawn of the transistor and the integrated circuit.

software packages for solving PDEs are that they cannot really handle large problems in an efficient manner, at least when it comes to general finite element solvers. The hinge is that it is fairly difficult to write a 'black box' solver (a solver that can handle a number of different problems and settings), that could solve large systems and in the same time be robust and reliable, which is a necessity for a commercial program. Large problems must be solved with iterative methods and this is non-trivial. Exploring and to some extent develop such methods is one of the major motivations for the present study. Another very important aspect of computing that also motivates this work is error control. Generally, this is only vaguely dealt with by commercial programs, possibly due to the complexity of the issue.

1.3.2. *Applications.* In industrial design of microdevices, in general, there is always the possibility to build prototypes and evaluate the device characteristics in experiments. However this is often a time consuming (expensive) and tedious process. This becomes more apparent when it comes to optimal design. The number of design parameters could be large and it would be impractical to find a good design through measuring on a number of different devices. With modern computer technology and appropriate models the design could be done by simulations, saving time and gaining efficiency in the design process. In this work we compute: **(*i*)** the fluid flow in microfluidic systems, and **(*ii*)** parameters (stability factors) characterizing the dynamics in microfluidic systems under realistic settings. This two points can be the basis for a computer assisted design procedure.

1.4. **Outline.** In the present work we focus on the part of the microfluidic system where the fluid mixing occurs and call this part of the system the *mixer*. In order to handle the problem theoretically and computationally we make the assumption that the mixer is a periodic device, in theory infinitely long. Due to the periodicity we can partition the mixer into small units called *unit cells*, see Figure 2.1. The complete dynamics of the mixer is contained in one unit cell and we therefore limit the study of the mixer to one of these unit cells.

The work is divided into three distinct but linked parts.

Eulerian view. Computing the flow in the unit cell in the Eulerian view. This should be done with error control. Since we have not established

any rigorous result in this direction and it is lacking in the literature we introduce the error control by a hypothesis that is likely to be valid and will be a subject for further studies.

Lagrangian view. Given the computed flow, a vector field u, we compute particle trajectories $x(t)$ by solving a system of ordinary differential equations (ODEs), $\dot{x}(t) = u(x)$ with $x(0) = x_0$. This is done with error control and the analysis is valid under the assumption of the hypothesis made for the error in the Eulerian view.

Stability. We consider the mixer as dynamical system and compute the stability factors for the system. These data are used to characterize the mixer and estimate the mixing time. Loosely speaking: the more unstable the system is, the better mixer it is.

1.4.1. *Basic assumptions.* We limit this work to the study of microfluidic systems such that the continuum hypothesis is valid which motivates the notion of fluid density and viscosity which are taken to be constant through this work. Under these conditions the incompressible Navier-Stokes equations will serve as a good model describing the fluid. Further assumptions are:

1. the no-slip boundary condition is valid,
2. Reynolds number $\mathrm{Re} < 10$,
3. Péclet number $\mathrm{Pe} > 100$,
4. the fluids considered are miscible and Newtonian.

We remark that these conditions are not particularly unique for microsystems. Hence, the results in this work are not only limited to microfluidics.

We illustrate the validation of the continuum hypothesis in an example. Considering a microfluidic system with water. The important microscopic timescale is the molecular collision time, *i.e.*, the average time between collisions for one molecule. Assuming that the thermal energy for one molecule equals its kinetic energy we obtain the velocity for one water molecule, $v = (2k_BT/m)^{1/2}$, where k_B is the Boltzmann constant, m is the molecular mass and T is the temperature. Furthermore, assuming that a mean free path equals the inter-molecular distance between water molecules, λ, gives an estimate for the molecular collision time $t_c = \lambda/v \sim 10^{-12}$ s. This is a lot smaller than any system timescales of interest, maybe $> 10^{-6}$ s. The size of a water molecule is $\sim 10^{-10}$ and the continuum hypothesis should be valid for any system $\gtrsim 10^{-7}$ m.

1.4.2. *Software and algorithms.* We discretize the Navier-Stokes equations by means of the finite element method and use the Dolfin library [34] as a basic platform for solving the problem. In addition a number of C++ classes have been implemented, *e.g.*, for matrix assembling, preconditioning and multigrid solvers. The initial grids were generated in FEMLAB and subsequent refinements were done in a MATLAB code. The ODE system and the stability factors were computed with the multi-adaptive ODE solver Tanganyika [48]. In addition we implemented a data acquisition class (interpolation from discrete to continuous data) based on a *binary space partitioning* algorithm.

2. Navier-Stokes equations and finite elements

We introduce the Navier-Stokes equations. For the physical background and a derivation we refer to the monograph [45] and for a mathematical analysis we refer to [13, 25, 49]. Assume $\Omega \subset \mathbf{R}^d, d = 2, 3$, is an open and bounded domain with Lipschitz continuous boundary. The stationary, or time-independent, Navier-Stokes equations in dimensionless form in Ω are,

$$\begin{aligned} -\nu\Delta u + (u \cdot \nabla)u + \nabla p &= f \quad \text{in } \Omega, \\ \nabla \cdot u &= 0 \quad \text{in } \Omega, \\ u &= g \quad \text{on } \partial\Omega, \end{aligned} \tag{2.1}$$

where u is the fluid velocity, p is the pressure, $f \in (H^{-1}(\Omega))^d$ is an external body force and $\nu = 1/\operatorname{Re}$. We also state the related linear Stokes equations,

$$\begin{aligned} -\nu\Delta u + \nabla p &= f \quad \text{in } \Omega, \\ \nabla \cdot u &= 0 \quad \text{in } \Omega, \\ u &= g \quad \text{on } \partial\Omega, \end{aligned} \tag{2.2}$$

with the same notation as for (2.1).

The incompressibility condition, $\nabla \cdot u = 0$, requires that the boundary value g in (2.1) and (2.2) satisfies

$$\int_{\partial\Omega} g \cdot n \, dS = 0,$$

where n is the outwards/inwards pointing unit normal at the boundary $\partial\Omega$. There are a number of such Dirichlet boundary conditions. In this work we will either use *confined flow*, that is, $g \cdot n = 0$ on $\partial\Omega$, or *pressure driven periodic channel flow*, that is, for a channel with a solid boundary (wall), Γ_{s}, and in/out flow boundaries $\Gamma_{\text{in}}/\Gamma_{\text{out}}$ that are identical in size and orientation,

$$\begin{aligned} u &= 0 \quad \text{on } \Gamma_s, \\ u|_{\Gamma_{\text{in}}} &= u|_{\Gamma_{\text{out}}}, \\ p|_{\Gamma_{\text{in}}} &= p|_{\Gamma_{\text{out}}} + R, \end{aligned}$$

where R is a constant representing the pressure drop over the channel segment. We call the domain inscribed by the boundaries Γ_{s}, Γ_{in} and Γ_{out} the *unit cell*, see Figure 2.1.

We remark that it is intrinsically difficult to assign in/out-flow boundary conditions; we have to know something about the solution before we even

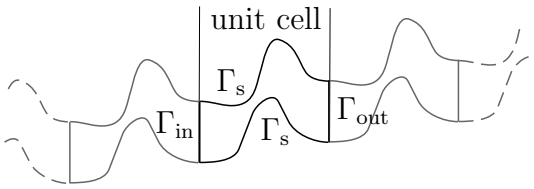

Figure 2.1: A periodic channel consisting of an infinite number of juxtaposed unit cells. The flow enters at the inflow boundary Γ_{in} and exits at the outflow boundary Γ_{out}. The inflow and outflow boundaries are identical in size and orientation. Solid boundaries such as channel walls are denoted by Γ_{s}.

have solved the problem. Assigning periodic boundary conditions resolves this difficulty in a neat way. For further details on consistent in/out-flow boundary conditions we refer to [53, 49].

2.1. **Weak formulation.** We state the weak formulation of the Navier-Stokes equations for the two types of boundary conditions that we will use. In the sequel we will use the following notation: the Sobolev space $W^{1,2}(\Omega) = H^1(\Omega)$; the modified L^2-space, $L^2_0(\Omega) = \{q \in L^2(\Omega) : \int_\Omega q\,dx = 0\}$, for the pressure; and the vector space

$$V(\Omega) = \{v \in H^1(\Omega) : \ v|_{\Gamma_{\text{s}}} = 0, \ v|_{\Gamma_{\text{in}}} = v|_{\Gamma_{\text{out}}}\},$$

for the periodic flow.

Confined flow. Find $(u, p) \in (H^1(\Omega))^d \times L^2_0(\Omega)$ such that $u = g$ on $\partial\Omega$ and,

$$\begin{aligned} \nu a(u, v) + c(u, u, v) + b(p, v) &= (f, v), \\ b(q, u) &= 0, \end{aligned} \tag{2.3}$$

for all $(v, q) \in (H^1_0(\Omega))^d \times L^2_0(\Omega)$. Setting $c(u, u, v) = 0$ we obtain the weak formulation for the Stokes equations.

Pressure driven periodic channel flow. Find $(u, p) \in (V(\Omega))^d \times L^2_0(\Omega)$ such that,

$$\begin{aligned} \nu a(u, v) + c(u, u, v) + b(p, v) &= (f, v) + R\ell(v), \\ b(q, u) &= 0, \end{aligned} \tag{2.4}$$

for all $(v, q) \in (V(\Omega))^d \times L^2_0(\Omega)$. Setting $c(u, u, v) = 0$ we obtain the weak formulation for the Stokes equations.

In the weak formulations above we use the notation,

$$\begin{aligned}
(u,v) &= \int_\Omega u_i v_i \, dx, \\
a(u,v) &= \int_\Omega \frac{\partial u_i}{\partial x_j} \frac{\partial v_i}{\partial x_j} \, dx, \\
b(p,v) &= -\int_\Omega p \nabla \cdot v \, dx, \\
c(u,v,w) &= \int_\Omega u_i \frac{\partial v_j}{\partial x_i} w_j \, dx, \\
\ell(v) &= \int_{\Gamma_{\text{in}}} v \cdot n \, dS,
\end{aligned}$$

with the usual summation convention, *i.e.*, $u_i v_i = \sum_{i=1}^d u_i v_i$.

2.2. **Finite element formulation.** Discretizing the weak formulations (2.3) or (2.4), that is, replacing the infinite-dimensional vector spaces $(H^1(\Omega))^d \times L^2_0(\Omega)$ for confined flows (or $(V(\Omega))^d \times L^2_0(\Omega)$ for periodic flows) with finite-dimensional approximations $(X_h(\Omega))^d \times M_h(\Omega)$ must be done with care. To begin with we assume that the domain Ω can be partitioned into a non-degenerate triangulation $\mathcal{T}$ [8]. In order for the discretization to be stable we have to choose $(X_h(\Omega))^d \times M_h(\Omega)$ such that the Babuska-Brezzi-Ladyzhenskaya (BBL) condition (or the inf-sup condition) is satisfied [9, 8]. There are many possible ways of choosing $(X_h(\Omega))^d \times M_h(\Omega)$ such that the BBL condition is satisfied. A family of vector spaces that are commonly used are the *Hood-Taylor* finite elements. These are vector spaces of continuous piecewise polynomials such that,

$$\begin{aligned}
X_h(\Omega) &= \{v_h \in C^0(\overline{\Omega}) \cap H^1(\Omega) : \ v_h|_K \in P_{n+1} \ \forall \, K \in \mathcal{T}\}, \\
M_h(\Omega) &= \{q_h \in C^0(\Omega) \cap L^2_0(\Omega) : \ q_h|_K \in P_n \ \forall \, K \in \mathcal{T}\},
\end{aligned} \tag{2.5}$$

where P_n denotes polynomials of degree $n \geq 1$. The stability of the Hood-Taylor elements for the three-dimensional Stokes equations was generally proven in [5].

We now discretize the weak form for the confined flow, equation (2.3), and obtain the corresponding finite element formulation. Find $(u_h, p_h) \in$

$(X_h(\Omega))^d \times M_h(\Omega)$ such that $u_h = I_h g$ on $\partial\Omega$ and,

$$\begin{aligned} \nu a(u_h, v_h) + c(u_h, u_h, v_h) + b(p_h, v_h) &= (f, v_h), \\ b(q_h, u_h) &= 0, \end{aligned} \tag{2.6}$$

for all $(v_h, q_h) \in (X_h(\Omega) \cap H_0^1(\Omega))^d \times M_h(\Omega)$. The I_h in the boundary condition is an interpolation operator. For the periodic flow the finite element formulation is similar and is obtained if we add $R\ell(v_h)$ to the right hand side of equation (2.6) and change the finite element spaces appropriately.

For the Stokes equations (2.2) the finite element formulation is obtained from (2.6) if we drop the non-linear part $c(u_h, u_h, v_h)$. Since we will refer to it later we state it explicitly. Find $(u_h, p_h) \in (X_h(\Omega))^d \times M_h(\Omega)$ such that $u_h = I_h g$ on $\partial\Omega$ and,

$$\begin{aligned} \nu a(u_h, v_h) + b(p_h, v_h) &= (f, v_h), \\ b(q_h, u_h) &= 0, \end{aligned} \tag{2.7}$$

for all $(v_h, q_h) \in (X_h(\Omega) \cap H_0^1(\Omega))^d \times M_h(\Omega)$.

Equation (2.6) is not readily solved due to the non-linearity $c(u_h, u_h, v_h)$. To proceed solving the problem we have to deal with this. The predominant method is to linearize, for example, $c(u_h, u_h, v_h) \approx c(u_h^{n-1}, u_h^n, v_h)$. With this particular choice of linearization we obtain a fixed point iteration scheme called the Oseen equations. With u_h^{n-1} known, find $(u_h^n, p_h^n) \in (X_h(\Omega))^d \times M_h(\Omega)$ such that $u_h = I_h g$ on $\partial\Omega$ and

$$\begin{aligned} \nu a(u_h^n, v_h) + c(u_h^{n-1}, u_h^n, v_h) + b(p_h^n, v_h) &= (f, v_h), \\ b(q_h, u_h^n) &= 0, \end{aligned} \tag{2.8}$$

for all $(v_h, q_h) \in (X_h(\Omega) \cap H_0^1(\Omega))^d \times M_h(\Omega)$. It is important to notice that this fixed point iteration scheme will converge when there is a unique solution to problem (2.1), see [23, p. 78]. We note that the Stokes equations are linear and hence, the finite element problem (2.7) is a linear algebra problem that could be solved accordingly.

Let $\{\phi_1, \ldots, \phi_{dM}\}$ be a basis for $(X_h(\Omega))^d$ and $\{\varphi_1, \ldots, \varphi_N\}$ be a basis for $M_h(\Omega)$. Then $u_h = u_i \phi_i$ and $p_h = p_j \varphi_j$ for constants u_i, $i = 1, \ldots, dM$

and p_j, $j = 1, \ldots, N$. With,

$$\begin{aligned} A_{ij} &= \nu a(\phi_i, \phi_j) + c(u_h^{n-1}, \phi_i, \phi_j), \\ B_{ki} &= b(\varphi_k, \phi_i), \\ F_i &= (f, \phi_i), \end{aligned}$$

we can write equation (2.8), and equally equation (2.7) by omitting the non-linear part in A and the iteration index n, in matrix form,

$$\begin{pmatrix} A & B^T \\ B & 0 \end{pmatrix} \begin{pmatrix} u^n \\ p^n \end{pmatrix} = \begin{pmatrix} F \\ 0 \end{pmatrix}. \tag{2.9}$$

This linear system of equations is often referred to as a discrete *saddle point problem*.

2.3. **Error estimates.** In this section we only consider the Stokes equations (2.2) with $g = 0$. For (u, p) solutions to the Stokes equations and (u_h, p_h) solutions to equation (2.7) where $(u_h, p_h) \in (X_h(\Omega) \cap H_0^1(\Omega))^d \times M_h(\Omega)$ such that the BBL condition holds, we have [9, p. 61]

$$||u - u_h||_{1,\Omega} + ||p - p_h||_{0,\Omega} \leq \inf_{v_h, q_h} (||u - v_h||_{1,\Omega} + ||p - q_h||_{0,\Omega}), \tag{2.10}$$

where the inf is taken over all $(v_h, q_h) \in (X_h(\Omega) \cap H_0^1(\Omega))^d \times M_h(\Omega)$ and where $||\cdot||_{m,\Omega}$ denotes the Sobolev norm in $H^m(\Omega)$. Below we will also use the corresponding seminorm $|\cdot|_{m,\Omega}$ where only the highest derivatives are taken into account. The estimate (2.10) particularly holds for the Hood-Taylor finite elements [5] and in the sequel we will assume that $(X_h(\Omega))^d \times M_h(\Omega)$ are the Hood-Taylor finite element spaces (2.5). Led by estimate (2.10) and the fact that the Hood-Taylor finite elements satisfies the BBL condition we can generalize Theorem 4.3 in [25, p. 181].

Theorem 2.1. *Let Ω be a bounded polygonal domain in $\mathbf{R}^d$ and let the solution (u, p) to the Stokes equations (2.2) with $g = 0$ be such that*

$$u \in (H^{k+1}(\Omega) \cap H_0^1(\Omega))^d, \qquad p \in H^k(\Omega) \cap L_0^1(\Omega),$$

for $1 \leq k \leq n + 1$, where n is as in (2.5). If the triangulation $\mathcal{T}$ is non-degenerate and such that: (i) if $d = 2$, no triangle has two sides on the boundary $\partial\Omega$; and (ii) if $d = 3$, every tetrahedron has at least one internal vertex. Then the solution $(u_h, p_h) \in (X_h(\Omega))^d \times M_h(\Omega)$ to equation (2.7) using the Hood-Taylor finite elements, satisfies the estimate

$$|u - u_h|_{1,\Omega} + ||p - p_h||_{0,\Omega} \leq C_1 h^k (|u|_{k+1,\Omega} + |p|_{k,\Omega}), \tag{2.11}$$

and if Ω *is convex or if the boundary is smooth,*

$$||u - u_h||_{0,\Omega} \leq C_2 h^{k+1}(|u|_{k+1,\Omega} + |p|_{k,\Omega}). \tag{2.12}$$

The proof is a mere formality when (2.10) is established.

Proof. For the interpolation operators, $I_h : H^{k+1}(\Omega) \cap H_0^1(\Omega) \to X_h(\Omega)$ for the velocity, and $I_h : H^k(\Omega) \cap L_0^1(\Omega) \to M_h(\Omega)$ for the pressure we get with (2.10) the estimate,

$$\begin{aligned} |u - u_h|_{1,\Omega} + ||p - p_h||_{0,\Omega} &\leq C|u - I_h u_h|_{1,\Omega} + ||p - I_h p_h||_{0,\Omega} \\ &\leq C_1 h^k(|u|_{k+1,\Omega} + |p|_{k,\Omega}), \end{aligned}$$

by Poincaré-Friedrichs inequality and standard interpolation estimates. Estimate (2.12) is obtained by a duality argument, which requires convexity or smoothness of the boundary $\partial\Omega$. □

This should to some extent motivate the use of higher order finite elements in microfluidic applications where the solution to the Stokes (and Navier-Stokes) equations is expected to be very regular.

2.3.1. *Maximum norm estimates.* Inspired by [19] we formulate a hypothesis estimating the *a priori* error in maximum norm.

Hypotheses 2.1. *For* Ω *convex,* (u, p) *and* (u_h, p_h) *as in Theorem 2.1. There is a constant* C *independent of* h *such that*

$$||u - u_h||_{0,\infty,\Omega} \leq Ch^{k+1}|\log h|^{\alpha}(|u|_{k+1,\infty,\Omega} + |p|_{k,\infty,\Omega}), \tag{2.13}$$

for $1 \leq k \leq n + 1$ *and some constant* α*.*

In [19] this was proven for $n = 1$, $d = 2$, and $\alpha = 3$.

3. Optimal solvers for the saddle point problem

We examine the discrete saddle point problem equation (2.9) in some more detail and introduce the more compact notation for the block-matrix,

$$\mathcal{A} = \begin{pmatrix} A & B^T \\ B & 0 \end{pmatrix}. \tag{3.1}$$

Generally, $\mathcal{A}$ is non-symmetric, indefinite, large and sparse and the submatrices are such that $A \in \mathbf{R}^{n\times n}$ and $B \in \mathbf{R}^{n\times m}$ with $n \geq m$. Typically, in this work $n + m \sim 10^6$, and the ratio of nonzero elements to zero elements is 10^{-4}. For finite element methods the number of unknowns in the linear system (2.9) scales as h^d, where h is the average finite element size. We note that this type of matrix occurs in other applications such as quadratic programming [28], and hence, is of more general interest.

With present computer technology it is certainly possible in many situation to refine the finite element triangulation until convergence for the laminar two-dimensional Navier-Stokes equations [70]. However, this is not always the case for the three-dimensional Navier-Stokes equations [71]. This is a direct consequence of the scaling mentioned above. The bottom line is that we will have to manage solving larger and larger linear systems in order to get three-dimensional problems to converge.

Solving large and sparse linear systems of equations we must rely on iterative methods. The time it will take to solve a linear system scales as N^α where N is the number of unknowns and α is an exponent related to the method ranging between 1 and 3. We have, $2 < \alpha \leqslant 3$ for direct solvers, *e.g.*, Gaussian elimination, and $\alpha \geq 1$ for multigrid solvers. If the time it takes to solve the linear system scales linearly with the number of unknowns ($\alpha = 1$), we say that the solver is *optimal*. Multigrid solvers are optimal for symmetric and positive definite problems whereas for non-symmetric and indefinite problems the efficiency may lack [7]. For further comments on multigrid and saddle point problems we refer to a recent review article [73].

Recently it was demonstrated that a solver combining a Krylov (iterative) method and multigrid can: **(*i*)** optimally solve the linear system arising from the finite element discretization of the two-dimensional Navier-Stokes equations [42], and **(*ii*)** efficiently solve the large linear system arising from the finite element discretization of the three-dimensional Navier-Stokes equations [71]. For these results a Krylov method is used

as a prime solver and the multigrid is employed in the preconditioning. There is a clear difference in how preconditioning is realized and therefore we choose to name the methodologies after their origin:

1. *The Anglo-Saxon preconditioner* due to Elman, Golub, Wathen, *et.al.*, [42, 21, 52].
2. *The German preconditioner* evolved from the DFG[5] high-priority research program *Flow Simulation with High-Performance Computers*, and due to Schäfer, Turek, Volker, *et.al.*, [68, 71].

In this work we extend the result in [42] demonstrating that the method works for three-dimensions. We now outline the over all idea in some more detail.

3.1. **The Anglo-Saxon preconditioner.** In the two very short papers [52, 36] it was shown that if the matrix $\mathcal{A}$ is preconditioned by the matrix,

$$\mathcal{P} = \begin{pmatrix} A & B^T \\ 0 & BA^{-1}B^T \end{pmatrix},$$

then the preconditioned matrix $\mathcal{P}^{-1}\mathcal{A}$ has at most three eigenvalues. Thus, a Krylov method applied to the preconditioned system will converge to the exact solution in less than four iterations. The matrix in the (2,2) position, $BA^{-1}B^T$ (the Schur complement), is however not readily computed and needs to be approximated. In [42] it was suggested and motivated to replace the Schur complement by $A_pF_p^{-1}M_p$ where A_p and F_p are the discretizations of the operators: $-\Delta$; and $-\nu\Delta + b\cdot\nabla$, where b is a convection field (u^{n-1} in the Oseen equations), and M_p is the pressure mass matrix. Put together in a right-preconditioned flexible GMRES algorithm [57, 58, 60] the method was shown to perform optimally, with only a mild dependence on the viscosity, solving a number of different two-dimensional Navier-Stokes problems. The inverse of $\mathcal{P}$ can be written as, replacing the Schur complement with $M_p^{-1}F_pA_p^{-1}$,

$$\mathcal{P}^{-1} \approx \begin{pmatrix} A^{-1} & 0 \\ 0 & I \end{pmatrix} \begin{pmatrix} I & B^T \\ 0 & I \end{pmatrix} \begin{pmatrix} I & 0 \\ 0 & M_p^{-1}F_pA_p^{-1} \end{pmatrix}. \tag{3.2}$$

In each cycle of the GMRES solver the action of this matrix must be computed. This is partitioned into computing the action of a number of sub-matrices: $(\boldsymbol{i})$ A^{-1} is computed by two V-cycles multigrid with symmetric point Gauss-Seidel smoothing, $(\boldsymbol{ii})$ A_p^{-1} is computed by two V-cycles

[5]Deutsche Forschungsgemeinschaft

multigrid but now with forward point Gauss-Seidel smoothing, and ***(iii)*** M_p^{-1} is computed by five iterations of preconditioned conjugate gradient [42].

3.2. **The German preconditioner.** If the matrix $\mathcal{A}$ is preconditioned by itself, *i.e.*, by $\mathcal{A}^{-1}$ then the problem is solved. Approximately computed, the inverse $\mathcal{A}^{-1}$ could be used as a right-preconditioner in a flexible GMRES algorithm. In [69, 70, 71] the action of the inverse of $\mathcal{A}$ was computed by multigrid and then used in a flexible GMRES solver. The method performed well solving a large scale three-dimensional benchmark Navier-Stokes problem. One of the difficulties in applying multigrid to saddle point problems is to find good smoothers. In the discussed work the authors suggested to employ a block Gauss-Seidel method.

3.3. **Implementation and verification.** In this work we chose to work with the P_2P_1 Hood-Taylor finite elements ($n = 1$ in (2.5) and in all the presented results the discrete saddle point problem (2.9) was solved with a method related to the Anglo-Saxon preconditioner. The preconditioner was implemented in a similar way as described in [42] although the conjugate gradient solver was replaced by a GMRES solver. The multigrid solver was implemented as a *multiple discretization multigrid* solver, *cf.* [71], this is due to the higher order finite element approximation of the velocity field. The initial grid was generated in FEMLAB and subsequently uniformly and regularly refined [3] two times. In Figure 3.1 we illustrate a typical grid at the finest level. The solver was stopped when the computed solution reached a tolerance of 10^{-6}.

3.3.1. *Optimality in 2D.* The implemented solver is optimal, *cf.* the introduction of this Section, when solving the two-dimensional Navier-Stokes equations [42]. We demonstrate this fact by solving the Navier-Stokes equations with $\nu = 1$ in the lid driven cavity problem on a number of different grids defined by four consecutive uniform refinements. In Figure 3.1 we plot the time it takes to solve the problem as a function of the number of unknowns, the degrees of freedom (*dof*). It is clear that the solver scales optimally, or very close to optimally. For a comparison we also solved the problem in FEMLAB 2.3 using a direct solver. In this case we only can present data from two refinements since the computer we used got out of memory after the third refinement. However, the trend is clear, compared with the implemented solver. ***(i)*** the FEMLAB solver does not

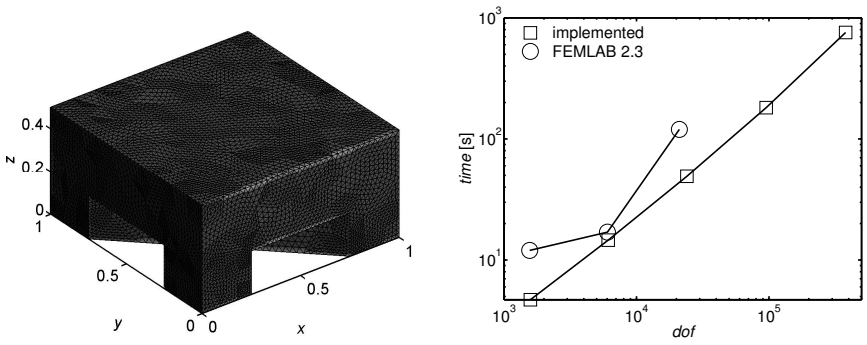

Figure 3.1: (left) The grid corresponding to the ridge mixer (see Paragraph 6.1), after two regular refinements which is the finest level in the multigrid hierarchy. There are 55277 nodes and 298432 tetrahedra. **(right)** The time for solving the two-dimensional Navier-Stokes equations with $\nu = 1$ in the lid driven cavity problem as a function of the degrees of freedom (*dof*). We compare the implemented solver with the FEMLAB 2.3 solver. For the FEMLAB solver the computer got out of memory after the third refinement.

scale optimally (which is not a surprise since we used a direct solver), ***(ii)*** the FEMLAB solver is slower than the implemented one, and ***(iii)*** the FEMLAB solver use more memory.

3.3.2. *Optimality in 3D.* For three-dimensional problems it is much more requiring to present results similar to the two-dimensional case. The size of the problems grows like h^d, *cf.* the discussion in the introduction of this Section. In this work we are only able to give 3D results for two consecutive refinements, limited by the hardware that was used. In Table 3.1 we present some results on the scaling for a number of 3D Stokes problems and one Navier-Stokes problem. We refer to Paragraph 6.1 for details on the different problems. From the results it seems plausible that the solver also is optimal for 3D problems but this is not conclusive at this momnet.

3.3.3. *Anglo-Saxon vs German preconditioning.* In the algorithms discussed in Paragraph 3.1 and 3.2 one or two multigrid V-cycles were applied in the

Table 3.1: The number of iterations (proportional to the time) for solving the three-dimensional Stokes and Navier-Stokes equations for four different problems (see Paragraph 6.1) as a function of the degrees of freedom (*dof*).

Mixer: RM, 3D Stokes			
dof	24061	173468	1314632
iter	31	32	33

Mixer: SHM, 3D Stokes			
dof	22207	156783	1173754
iter	37	37	41

Mixer: dSHM, 3D Stokes			
dof	22272	155863	1160914
iter	45	47	47

Mixer: MM, 3D NS Re=10			
dof	21786	157182	1191916
iter	119	122	129

preconditioning. These particular choices seem to be empirically established. For this reason we may ask for a rigourously motivated stopping criterion. We have not found such criterion in the literature.

It would be interesting to compare the discussed preconditioner on a set of benchmarks problems. We have tried to achieve results in this direction but we were not able to obtain conclusive and 'fair' results. This was partly because all the implementations were made on a sequential computer whereas it seems necessary to implement the German preconditioner on a parallel computer, where the block Gauss-Seidel smoother should work well.

4. Mixing in microfluidic channels

In the introduction, Paragraph 1.1.1, it was pointed out that the combination of small Reynolds number $\mathrm{Re} < 10$ (possibly $\ll 10$) and large Péclet number $\mathrm{Pe} > 100$ is significant for many microfluidic systems. As a consequence it is difficult to mix fluids in these systems. For small Reynolds numbers there is no turbulence and we cannot rely on such inertial effect for mixing, and for large Péclet numbers convective effects will dominate diffusive effects and mixing by diffusion will be a relatively slow process.

We consider stationary flow in channels with characteristic length L, the diameter (width) of the channel, and characteristic velocity U, the maximum flow velocity along the channel. The objective is to mix two miscible fluids, A and B, that enter in a Y-junction. If the geometry of the channel is such that a parabolic velocity profile is maintained along the channel there will be little mixing and only due to diffusion. This has been demonstrated in several papers, *e.g.*, [37, 40, 43] and we illustrate it in Figure 4.1. To enhance the mixing the idea is to introduce convection in the cross section of the channel. In any case we would like the time it takes to mix the two fluids, t_m, the *mixing time*, to be as small as possible.

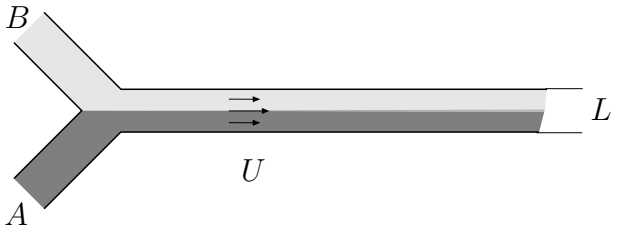

Figure 4.1: A Y-junction. Fluids A and B are entering the channel in a Y-junction. In microfluidics the characteristic length L, the width of the channel and the characteristic velocity U, the maximum velocity, are both small. Inertial effects are weak and if the channel is smooth the two fluids will flow along next to each other. There will be little mixing and only due to diffusion.

Inspired by the general definition of *strong topological mixing* in [54, p. 118] we now define mixing in periodic channels (mixers). Let $x(t) = X(t, t_0; x_0)$ be the solution to the ODE $\dot{x} = u(x)$ with $x(t_0) = x_0$, where u

is the velocity field in the channel. We consider one unit cell and denote the inflow boundary of the unit cell by Γ. Remembering that the inlet and outlet boundaries are equivalent due to the periodicity we introduce the mapping $T : \Gamma \to \Gamma$ defined by $T(x) = X(t_1, t_0; x)$ for t_1 such that $X(t_1, t_0; x)$ is on the outflow boundary of the unit cell. We assume that there is no fixed points in the unit cell or other features that might trap a trajectory in the unit cell. Let $T^n(x) = T \circ T^{n-1}(x)$ with $T^0(x) = x$. The mapping T^n is called the Poincaré mapping of the channel flow $X(t, t_0; x)$.

Definition 4.1. (*Strong topological mixing in periodic channels*) We say that a periodic channel flow mixes if for any two non-empty subsets of Γ, A and B, there is an N such that $T^n(A) \cap B \neq \emptyset$ for any $n > N$.

We note that if the mapping T is such that it meets the requirements of strong topological mixing then T is *topologically transitive* in dynamical system theory language. The definitions for strong topological mixing and topological transitive are equivalent.

4.1. **Mixing by diffusion.** We consider a situation were there is no convection in the channel cross section. Any initial configuration of miscible fluids will mix, homogenize, in time due to diffusion. The maximum time this will take is approximately the time it will take for one molecule/particle to diffuse over the channel cross section. This can be estimated by the *Einstein relation*,

$$t_m = \frac{L^2}{D}, \tag{4.1}$$

where D is the diffusion coefficient, see Paragraph 1.1.1. Relating this time to the mean flow velocity U gives us a distance along the channel, the *mixing length*, $\Delta x_m = UL^2/D = \mathrm{Pe}\, L$. For some combinations of the parameters U, L and D, that are common in microfluidics, the mixing time (or equivalently the mixing length) is unpractically large. We illustrate this in Figure 4.2.

4.2. **Mixing by chaotic convection.** We consider a situation were there is no diffusion in the channel or very little diffusion. From every day practice we sort of know that such a system will mix if we stir it. This idea was theoretically worked out in detail during the eighties [2, 1, 54], and it is commonly referred to as *chaotic advection*. The main idea is that dynamical systems that are chaotic will mix. There are many definitions of

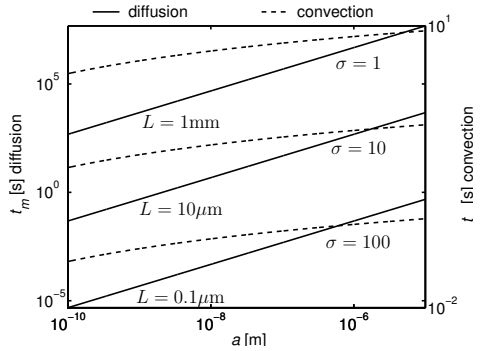

Figure 4.2: Mixing time, t_m, as function of molecule/particle size a in water. The **left** y-axis gives the mixing time by diffusion, and is based on the Einstein relation (4.1), for $L = (10^{-7}, 10^{-5}, 10^{-3})$ m; and the **right** y-axis gives the mixing time by chaotic convection, base on relation (4.2) rewritten to $t_m = 1/(2\sigma)\ln(LU/D)$, where the diffusion coefficient is $D = k_B T/(6\pi\eta a)$, and for $\sigma = (1, 10, 100)$ assuming $\text{Re} = 1$ and $\mu = 10^{-6}$ (water).

chaos in dynamical systems in the literature. Led by the simple definition in [17, p. 50], we choose a definition that will serve our purposes using the notation introduced for Definition 4.1. Before the actual definition of chaos in periodic channel flows we give two additional definitions that will define the notation necessary, these are also inspired by [17, p. 49].

Definition 4.2. The flow $X(t, t_0; x) : \Omega \to \Omega$ has sensitive dependence on initial conditions if there exist $\delta > 0$ such that, for any $x \in \Omega$ and any neighborhood N of x, there exist $y \in N$ and $t > t_0$ such that $||X(t, t_0; x) - X(t, t_0; y)|| > \delta$.

Definition 4.3. The point x is a periodic point of period n if $T^n(x) = x$.

Definition 4.4. (*Chaos in periodic channel flow*) The flow $X(t, t_0; x)$ is said to be chaotic if,

1. $X(t, t_0; x)$ has sensitive dependence on initial conditions,
2. T is topologically transitive,
3. periodic points of T are dense in Γ.

We will use item (1) in the definition to estimate the mixing time by chaotic convection. We assume $X(t, t_0; x)$ to be chaotic and to have an exponential growth of small perturbations ℓ_0, *i.e.*, $\ell_0 \exp(\sigma t)$, for $\sigma > 0$.

In practice there is always diffusion and we denote the distance over which diffusion have to go in order to reach mixing by Δr. Due to the chaotic convection we assume that this distance will decrease with time as $\Delta r = L - \ell_0 \exp(\sigma t)$ where we assume $\ell_0 \ll L$. Led by the Einstein relation for the diffusion time we choose $\ell_0 = (t_0 D)^{1/2}$ and $t_0 = L/U$ the characteristic time for the flow. We say that the system is mixed when $\Delta r = 0$ and get an estimate for the mixing time,

$$t_m = \frac{1}{2\sigma} \ln(\mathrm{Pe}). \tag{4.2}$$

Here we have used $\ell_0/L = (D/LU)^{1/2} = \mathrm{Pe}^{-1/2}$ and we note that $\ell_0 \ll L$ for large Péclet numbers. Hence, t_m grows slowly with Pe. For fixed Re and σ we plot the mixing time as a function of the particle diameter a (remembering that $D = k_B T/(6\pi\eta a)$, see Paragraph 1.1.1). We illustrate this in Figure 4.2 for $\mathrm{Re} = 1$. For consistency we also give the mixing length in this case, $\Delta x_m = U/(2\sigma) \ln(\mathrm{Pe})$.

We note that item (2) in Definition 4.4 is identical with Definition 4.1 for mixing. Thus, chaos implies mixing. Item (3) seems not to be important for characterizing mixing, we included it for completeness.

5. Stability in computed flows

We consider the system of ODEs,

$$\dot{x} = u(x), \quad t \in (t_0, T],\ x(t) \in \Omega; \quad x(t_0) = x_0, \tag{5.1}$$

where u is the velocity field defined by the Navier-Stokes equations (2.1) or the Stokes equations (2.2). We would like to predict the stability of such systems in terms of the dependence on initial conditions, item (1) in Definition 4.4. Therefore we introduce the perturbed problem,

$$\dot{\bar{x}} = u(\bar{x}), \quad t \in (t_0, T],\ \bar{x}(t) \in \Omega; \quad \bar{x}(t_0) = \bar{x}_0, \tag{5.2}$$

and subtract it from equation (5.1). With $e = x - \bar{x}$ and $e_0 = x_0 - \bar{x}_0$ small, we get,

$$\dot{e} = A(t)e, \quad t \in (t_0, T]; \quad e(t_0) = e_0, \tag{5.3}$$

where $A(t) = \int_0^1 Du(\bar{x}(t) + se(t))\, ds$ and Du is the Jacobian. We assume that $u(x) \in W^{1,\infty}(\Omega)$ which implies that the matrix $A(t)$ is bounded, *i.e.*, $\sup_t ||A(t)|| < \infty$. Equation (5.3) is the linear nonautonomous system frequently studied in dynamical system theory. The traditional analysis of these systems relates to characteristic exponents and particularly to Lyapunov exponents. Below we give account for these concepts and refer for further details to a recent review article [18].

5.1. **Lyapunov exponents.** Let $X(t)$ be a fundamental matrix solution to (5.3), *i.e.*, a solution for $\dot{X} = A(t)X$. The characteristic exponents, with $\varphi_i \in \mathbf{R}^d$ the ith unit vector,

$$\lambda_i = \limsup_{t\to\infty} \frac{1}{t} \ln ||X(t)\varphi_i||, \qquad i = 1, \ldots, d,$$

are called the *Lyapunov* exponents when $\sum^d \lambda_i$ is minimized with respective to all possible fundamental matrix solutions. The Lyapunov exponents characterize the asymptotic behavior of solutions to (5.3).

5.2. **Stability factors.** Consider the dual problem to (5.3),

$$-\dot{z} = A^*(t)z, \quad t \in (t_0, T]; \quad z(T) = z_T, \tag{5.4}$$

where A^* is the adjoint to A, $T > t_0$ and with arbitrary data $z_T \in \mathbf{R}^d$. Taking the scalar product of (5.3) and z, and the scalar product of (5.4)

and e we get

$$(\dot{e}, z) - (Ae, z) = 0,$$
$$-(e, \dot{z}) - (e, A^*z) = 0,$$

where $(\cdot, \cdot)$ is the euclidian scalar product in $\mathbf{R}^d$. Subtracting these equations we get the differential equation $D_t(e, z) = 0$, with the solution,

$$(e(T), z_T) = (e_0, z(t_0)) = (e_0, X^*(t, T)z_T), \tag{5.5}$$

where the matrix $X^*(t, T)$ is the solution operator to the dual problem (5.4). Choosing $z_T = \varphi_i$, the unit vectors, we define the *stability factors* $s_{ij}(t_0, T) = |(X^*(t_0, T)\varphi_i)_j|$ and $s_i(t_0, T) = ||X^*(t_0, T)\varphi_i||$. With $z_T = \varphi_i$ in (5.5) we get the estimate,

$$|e_i(T)| \leq ||e_0||s_i(t_0, T). \tag{5.6}$$

There are a few differences between stability factors and Lyapunov exponents. For a system of three coupled ODEs there are nine stability factors whereas only three Lyapunov exponents, hence the stability factors will give more detailed information of the dynamics in the dynamical system. The stability factors could also describe any growth, *e.g.*, polynomial or exponential whereas the Lyapunov exponents only captures exponential growth. The stability factors describe the initial behavior whereas the Lyapunov exponents describe the asymptotic behavior as $t \to \infty$.

5.3. **Error estimates in computed flow trajectories.** Substituting u in (5.2) with a computed velocity field u_h we get,

$$\dot{\bar{x}} = u_h(\bar{x}), \quad t \in (t_0, T],\ \bar{x}(t) \in \Omega; \quad \bar{x}(t_0) = \bar{x}_0. \tag{5.7}$$

Subtracting (5.7) from (5.1) we get the ODE for the error, $e = x - \bar{x}$,

$$\dot{e} = A(t)e + E(t), \quad t \in (t_0, T]; \quad e(t_0) = e_0, \tag{5.8}$$

where $A(t)$ as in (5.3) and $E(t) = u(\bar{x}) - u_h(\bar{x})$.

In the same way as in Paragraph 5.2 we introduce the dual problem to (5.8), subtracting the weak forms and solving the resulting differential equation. We get,

$$(e(T), z_T) = (e_0, z(t_0)) + \int_{t_0}^{T} (E(t), z(t))\, dt,$$

and with $z_T = \varphi_i$ we get the estimate,

$$|e_i(T)| \leq ||e_0||s_i(t_0, T) + \max_{t_0 \leq t \leq T} ||E(t)||S_i(t_0, T),$$

where $S_i(t_0, T) = \int_{t_0}^{T} ||X^*(t, T)\varphi_i||\, dt$ is another stability factor. Finally, with Hypothesis 2.1 we get,

$$|e_i(T)| \leq ||e_0|| s_i(t_0, T) + Ch^{k+1} S_i(t_0, T),$$

assuming that the finite element approximation for the velocity field is of order k, and C is a constant depending on $|u|_{k+1,\infty,\Omega}$ and $|p|_{k,\infty,\Omega}$.

6. Channel mixers: A case study

The design of passive (no use of external stimuli) microfluidic mixers with good mixing properties for small Reynolds numbers, roughly $Re < 10$, is a fairly recent problem that only has been addressed in a few studies, see [61, 46, 63, 43]. Additional work that relate to these studies may be to systematically optimize the proposed mixers but also to devise new designs that do not necessary rely on mechanisms known from macroscopic mixers, see for example [56]. In this work we study mixers related to: **(*i*)** channels patterned with ridges or staggered herringbones [61]; **(*ii*)** serpentine, or meandering channels [46, 63]; and **(*iii*)** combination of the two. Below we outline the design of a number of mixers and briefly discuss parameters that should be recognized in optimal design of the mixers, something that we have not done in this work. The mixers are meant to be archetypical in design and in this way capture main features of different mixers. It is important to realize that the designs we use in this study have been limited by the fact that the flow in the device should be computable, with reasonable accuracy.

6.1. **Parameters and design.**

6.1.1. *Ridge and herringbones mixer.* Patterning the bottom of a straight rectangular channel with periodic structures, ridges or herringbones, will induce flow perpendicular to the main flow direction. This was demonstrated and experimentally studied in [61]. Led by these results we define three different mixers:

1. the *ridge mixer* (RM),
2. the *staggered herringbone mixer* (SHM),
3. the *dense staggered herringbone mixer* (dSHM),

all depicted in the Figures 6.1 and 6.2.

For optimal design of the mixers we recognize a few parameters that should be important to tune: **(*1*)** the angle θ, **(*2*)** the number α, controlling the depth of the structures, **(*3*)** the number β, controlling the size of ridges/herrigbones along the channel and the distance between the structures, **(*4*)** the width w and the length ℓ, and **(*5*)** the number p, controlling the asymmetry in the herringbone structures. The choice $\theta = 45°$, and $p = 2/3$ was motivated in [61] with a simplified analytical argument. However, the actual optimal values for all the parameters, including θ and p, remain unknown.

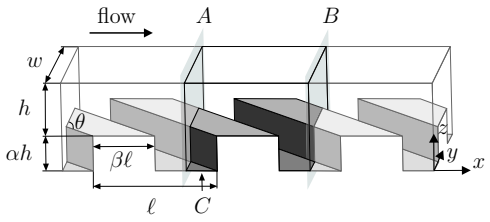

Figure 6.1: The ridge mixer (RM). The unit cell is defined by the partitioning planes A and B. In the simulations we choose the following values of the parameters: $\ell = w = 1$, $h = 0.3$, $\theta = 45°$, $\alpha = 2/3$, $\beta = 0.5$, and the length of the unit cell is $= 1$.

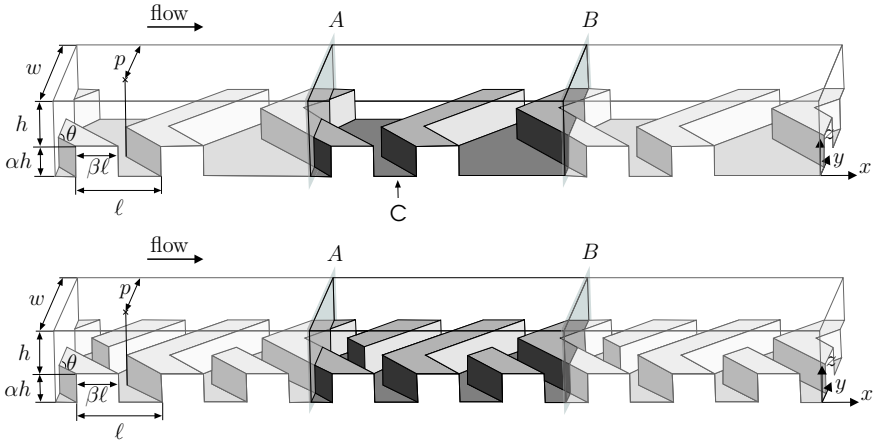

Figure 6.2: (top) The staggered herringbone mixer (SHM). **(bottom)** The dense staggered herringbone mixer (dSHM). The unit cell is defined by the partitioning planes A and B. In the simulations we choose the following values of the parameters: $\ell = 2/3$, $w = 1$, $h = 1/5$, $\theta = 45°$, $\alpha = 2/3$, $\beta = 3/8$, $p = 2/3$, and the length of the unit cell is $= 14/9$.

6.1.2. *Meandering channel mixers.* In curved channels a secondary flow will appear in the channel cross section when the Reynolds number is sufficiently large. This secondary flow is due to a centrifugal instability and is called *Dean flow* [56]. Relying on such inertial effects, a channel

mixer may be devised by a meandering (MM) [63] or serpentine [46] kind of design.

6.1.3. *Combinations.* We may try any combination of the mixers suggested above. In the combined mixer (CM) we explore the idea of triggering inertial effects by introducing ridge-like obstacles in a meandering channel.

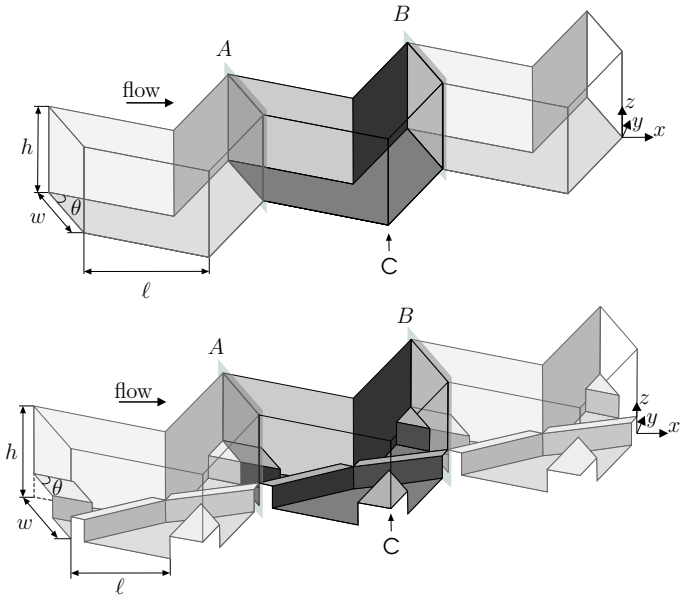

Figure 6.3: (top) The meandering mixer (MM). **(bottom)** The combined mixer (CM). The unit cell is defined by the partitioning planes A and B. In the simulations we choose the following values of the parameters: $h = \ell = w = 1$, $\theta = 45°$, and the length of the unit cell is $= 2$.

6.2. **Simulations.** The structure of the velocity field of the ridge mixer (RM) and herringbone mixers (SHM, dSHM) does not change much with the Reynolds number with in the range considered $\mathrm{Re} \leq 10$. This is in agreement with experimental observations [61]. However, for the meandering mixers, where the mixing mechanism relies on inertial effects, we see that the Dean vortices start to appear at $\mathrm{Re} \gtrsim 10$. This observation really questions the use of meandering mixers for microfluidic applications and consequently we will only present a few results on this type of mixer.

Table 6.1: We compare the ratio of the maximum flow velocity along the channel to the maximum transverse flow velocity in the cross section C, in Figures 6.4–6.7.

mixer	$\max u_1 / \max u_2$	$\max u_1 / \max u_3$
RM, Stokes	5	4
SHM, Stokes	3	4
dSHM, Stokes	3	4
MM, NS Re = 1	77	207
MM, NS Re = 10	8	26
CM, NS Re = 1	41	9
CM, NS Re = 10	10	11

6.2.1. *Euler flow fields.* In Figures 6.4–6.7 we illustrate the flow field in the studied mixers. These pictures give a good feel for how the mixer will work. The ridge mixer(RM) will merely rotate the fluid in the cross section of the channel and the dynamics of the flow is related to the dynamics in the two or three-dimensional lid driven cavity flow. Since the lid driven cavity flow is known for its *weak reorientation* properties [54, page 73], and hence poor mixing properties, we may anticipate the same for the ridge mixer. For the staggered herringbone mixers we can see two vortices in the cross section. The position of these vortices will change continuously along the channel resulting in a flow field that will have good mixing properties. We note that these observations were already made in [61].

Together with the illustrated flow fields Figures 6.4–6.7 and the discussion above we may also characterize the properties of the mixer by computing the ratio of the maximum flow velocity along the channel, in the x-direction, to the maximum flow velocity in transverse directions, the y and z-directions, in the cross sections marked with C in Figures 6.4–6.7. A small ratio indicates that there will be large mass transport in the cross section, which could be favorable for mixing. We present such data in Table 6.1. We note that for the meandering mixer (MM) with Re = 1 and Re = 10 the ratio is large compared to the ridge and herringbone mixers, which indicates that the mixer will not be efficient for Re $\leq$ 10. For the

combined mixer (CM) we observed no major improvements in the direction of the idea we had for this kind of design, *i.e.*, that the an obstacle should trigger inertial effects.

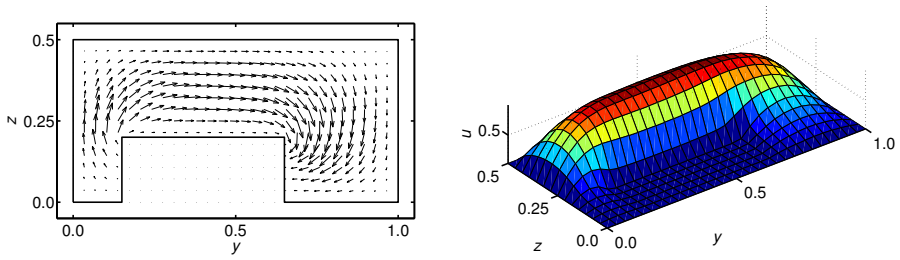

Figure 6.4: The ridge mixer (RM). Velocity field for the Stokes equations in the cross section of the channel at position C in Figure 6.1. **(left)** The y and z velocity field. **(right)** The x velocity field.

6.2.2. *Stability factors.* A quantitative measure of the flow character is given by the stability factors $s_i(t) = s_i(0,t)$ (with the initial time $t_0 = 0$), see Paragraph 5.2. We would like to predict wether the flow is chaotic and if it is we would like to know how strongly chaotic it is. For fixed initial data, a point x_0, we compute a sequence of stability factors, $s_i(t)$

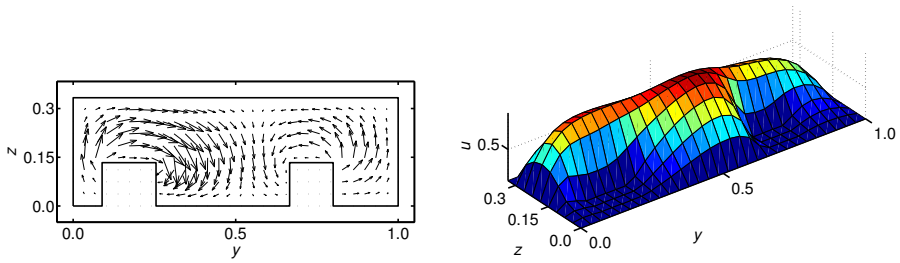

Figure 6.5: The dense staggered herringbone mixer (dSHM). Velocity field for the Stokes equations in the cross section of the channel at position C in Figure 6.2 bottom. **(left)** The y and z velocity field. **(right)** The x velocity field. We remark that the flow field in the staggered herringbone mixer (SHM) is similar in structure to the depicted flow field.

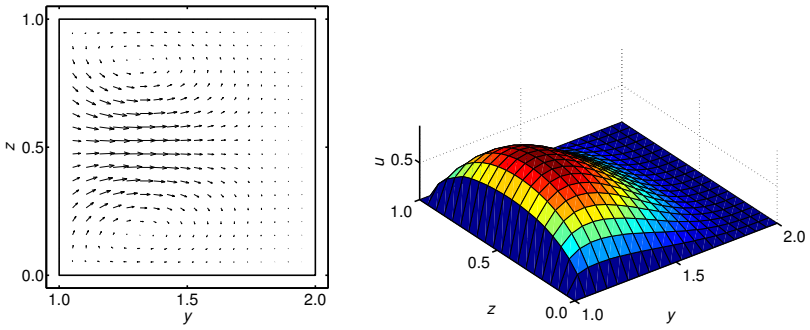

Figure 6.6: The meandering mixer (MM). Velocity field for the Navier-Stokes equations, for Re = 10, in the cross section of the channel at position C in Figure 6.3 top. **(left)** The y and z velocity field. **(right)** The x velocity field. We remark that for Re $\lesssim 1$ there is nearly no y and z velocity field in the cross section at position C, *cf.* Table 6.1.

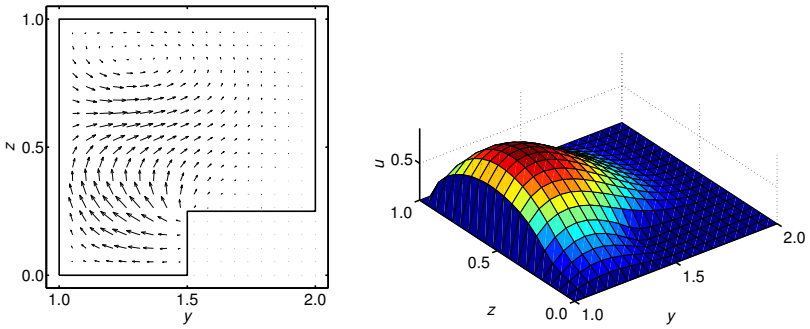

Figure 6.7: The combined mixer (CM). Velocity field for the Navier-Stokes equations, for Re = 10, in the cross section of the channel at position C in Figure 6.3 bottom. **(left)** The y and z velocity field. **(right)** The x velocity field.

and with the ansatz $s_i(t) = \exp \sigma_i t$ we estimate σ_i by fitting the data, see Figure 6.8. Note that we are not limited to exponential growth, we could make any other ansatz, *e.g.*, polynomial. The σ_i is a number that describes how perturbations will grow in the flow. This value could be used in (4.2) estimating the mixing time in the flow. In Table 6.2 we account for the exponent σ_i, for different mixers and different initial data,

x_0. We note that the numbers are given in dimensionless form and should be multiplied with the inverse of the characteristic time $t_0^{-1} = U/L$ before applied in (4.2). There is some variation in σ_i as a function of x_0 and we can not conclude that the flow is equally chaotic over the cross section. This point needs to be worked out in more detail.

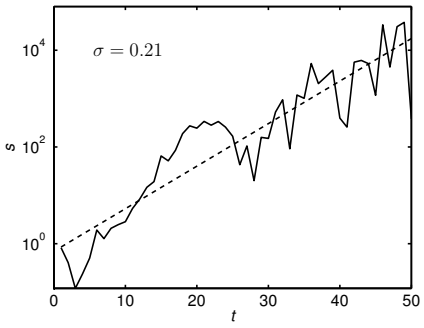

Figure 6.8: The stability factor, the solid line, $s_1(t)$ computed in the dense staggered herringbone mixer (dHSM) for the initial data $x_0 = (0.01, 0.5, 0.2)$. The stability factor range over five orders of magnitude and it seem plausible that the growth is exponential. From the fitted data, the dashed line, we deduce that $\sigma_1 = 0.21$.

6.2.3. *Flow trajectories and Poincaré mappings.* Flow mixes if it has the property in Definition 4.1, which is equivalent to the flow being topologically transitive. A qualitative measure for this is the Poincaré mapping or, equally but more detailed, the projection of a flow trajectory onto the yz-plane, the cross section. Ideally, for the flow to be topologically transitive, we like to see the Poincaré sections spread out over the entire yz-cross section. To recognize such behavior it is necessary to compute the Poincaré sections in a larger time interval. This is intrinsically difficult for two reasons: ***(i)*** the dynamical system is likely to have sensitive dependence on initial conditions, ***(ii)*** a computed velocity field is used for computing the flow trajectories, introducing additional errors in the computation. For these reasons we only plot the initial behavior. In Figure 6.9 we have plotted the yz-projection of two particle trajectories, one from the ridge mixer and the other from the dense staggered herringbone mixer. From the plots

Table 6.2: Exponents for the stability factors. The results are obtained from fitting computed stability factors to the ansatz $s_i(t) = \exp \sigma_i t$. The exponents are in dimensionless form, i.e, $\sigma_i = t_0 \sigma_i'$ where $t_0 = L/U$ is the characteristic time and the σ_i' has the dimension [1/s]. For the meandering mixer the results are tentative, the computed stability factors only range over two orders of magnitude and we can not really rely on the fitted data.

Mixer: RM, 3D Stokes

x_0	σ_1	σ_2	σ_3
$(0.0, 0.2, 0, 4)$	0.10	0.10	0.10
$(0.0, 0.3, 0, 4)$	0.06	0.07	0.07
$(0.0, 0.4, 0, 4)$	0.06	0.05	0.07
$(0.0, 0.5, 0, 4)$	0.07	0.07	0.06

Mixer: SHM, 3D Stokes

x_0	σ_1	σ_2	σ_3
$(0.0, 0.2, 0, 2)$	0.05	0.04	0.05
$(0.0, 0.3, 0, 2)$	0.04	0.06	0.06
$(0.0, 0.4, 0, 2)$	0.12	0.10	0.09
$(0.0, 0.5, 0, 2)$	0.07	0.07	0.07

Mixer: dSHM, 3D Stokes

x_0	σ_1	σ_2	σ_3
$(0.0, 0.2, 0, 2)$	0.19	0.19	0.14
$(0.0, 0.3, 0, 2)$	0.15	0.18	0.14
$(0.0, 0.4, 0, 2)$	0.10	0.07	0.06
$(0.0, 0.5, 0, 2)$	0.21	0.20	0.21

Mixer: MM, 3D NS, Re = 10

x_0	σ_1	σ_2	σ_3
$(0.0, 0.5, 0, 05)$	*0.03*	*0.02*	*0.02*

we can see that the flow in the ridge mixer merely rotates the fluid whereas for the herringbone mixer the reorientation seems to be more random-like.

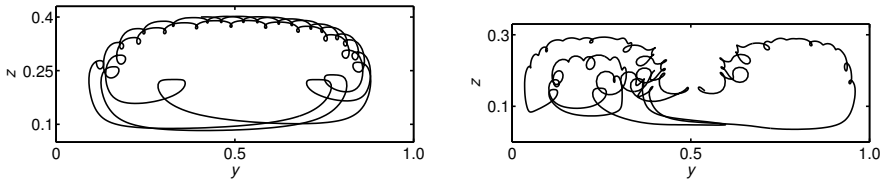

Figure 6.9: Projection of flow trajectories onto the yz-plane, the cross section of the channel. **(left)** The ridge mixer (RM) with $x_0 = (0.0, 0.5, 0.4)$ **(right)** The dense staggered herringbone mixer (dSHM) with $x_0 = (0.0, 0.5, 0.2)$, a similar result is obtained for the (SHM).

6.3. **Summary.** Evaluating the mixing properties of a mixer it is important to recognize items (1) and (2) in Definition 4.4 where item (2) guarantees that the mixer will mix fluids and item (1) with equation (4.2) will give an estimate for the time it will take to obtain mixing. The mixing time is readily computed as was demonstrated in the paragraphs above. However, it is much more difficult to prove or by other quantitative means establish item (2) for a mixer in realistic settings. We could plot the Poincaré mapping or equivalent and in this way gain qualitative results indicating that the dynamical system defined by the mixer is topologically transitive, *i.e.*, satisfying the criteria in Definition 4.1 and hence will mix.

For the ridge and herringbone mixers we could conclude that the herringbone mixers, SHM and dSHM with similar properties, are better mixers in terms of items (1) and (2) in Definition 4.4. The meandering mixer does not seem to work for $\mathrm{Re} \lesssim 10$ and we conclude that this design principle is not suited for microfluidic applications.

7. Outlooks: particle models

Overlooked in this study is that many microfluidic applications comprise fluids with solved large molecules or particles, collectively called *colloidal dispersions*. It is well known that the hydrodynamical interaction between particles will have a major influence on the flow characteristics. Resolving the complex hydrodynamical particle interactions in colloidal dispersions necessitate a methodology where the motion of the fluid and colloids are fully coupled. It is possible to take this into account in a *Direct Numerical Simulation* and there are a number of such methods. In the Stokesian dynamics [6, 24] inertial effects are ignored and the method gives good results at very small Reynolds numbers and therefore it is strictly valid only for $\mathrm{Re} = 0$. Moreover, only the two-body problem can be treated in an exact manner [38, 39], and hence Stokesian dynamics is lacking in the treatment of the resistance tensor, *i.e.*, in how the important hydrodynamic interaction is dealt with. It is also limited to spherical particles.

For finite Reynolds number a number of different methods have been proposed in recent years, see, *e.g.*, the special issue on multiphase flows in Computational Physics, 169, 2001. Finite elements are commonly used as a core technique and the problems are addressed as moving boundary problems. One fundamental issue is the adjustment of the mesh to the moving boundaries of the particles. In the Arbitrary Lagrange-Euler technique [35], the mesh is deformed along the moving particles. This requires regeneration of the mesh as it deteriorates. In the Distributed Lagrangian Multiplier technique [27] computations are done on a fixed mesh and the rigid body motion of the particles is enforced by introducing Lagrange multipliers. We also mention the Front Tracking Finite Difference technique [67] and the Lattice Boltzmann technique [44] based on microscopic models.

In a typical microfluidic application were a colloidal dispersion is considered the number of particles will be fairly small and it should be ideal to address the problem by a direct numerical simulation.

7.1. **A boundary value problem.**

A colloidal dispersion can be described by a well-posed boundary value problem, see for example [27]. We assume that the fluid carrying the colloids is Newtonian and can be described by the incompressible Navier-Stokes equations and that the dispersed colloids translate and rotate according to a set of coupled Langevin-Euler equations. The Navier-Stokes equations and the Langevin-Euler

equations are coupled through hydrodynamical and Brownian forces acting on the interface between the fluid and the colloids. We denote the domain of the body containing the whole system by $\Omega \subset \mathbf{R}^d$ where $d = 2, 3$ and the time dependent domains of the colloids by $B_j(t)$, where $j = 1, \ldots, N$ and N is equal to the total number of colloids. Note that the shape of the colloids can be arbitrary. The Navier-Stokes equations (time dependent) are solved in the domain $\Omega \setminus \cup_{j=1}^{N} B_j(t)$.

The no-slip boundary condition on the colloids reads,

$$u(x,t) = V_j(t) + \omega_j \times (x - G_j(t)), \quad x \in \partial B_j(t),$$

where $V_j(t)$ denotes the velocity, and $\omega_j(t)$ and the angular velocity, of the center of mass $G_j(t)$ of the j:th colloid.

The colloids translate and rotate in the fluid according to the Langevin-Euler equations,

$$M_j \frac{dV_j}{dt} = F_j^{\text{ext}} + F_j^{\text{hyd}} + F_j^{\text{brw}} + \sum_{i,i\neq j}^{N} F_{ij}^{\text{col}},$$

$$I_j \frac{d\omega_j}{dt} + \omega_j \times I_j \omega_j = T_j^{\text{hyd}} + T_j^{\text{brw}},$$

where M_j is the mass and I_j is the inertia tensor of the j:th particle. F_j (T_j) denote various types of forces (torques) acting on the j:th colloid. They are distinguished by the following superscripts:

ext: External forces, *e.g.*, gravity or electromagnetic forces.

hyd: Hydrodynamical force on the j:th colloid,

$$F_j^{\text{hyd}} = -\int_{\partial B_j} \sigma n \, dS,$$

where σ is the stress tensor, and the torque at G_j of the hydrodynamical forces acting on the j:th colloid,

$$T_j^{\text{hyd}} = -\int_{\partial B_j} (x - G_j(t)) \times \sigma n \, dS.$$

brw: Brownian forces (torques) exerted by the fluid on the particles; these will be of stochastic nature and characterized by,

$$\langle F_j^{\text{brw}} \rangle = 0, \qquad \langle F_j^{\text{brw}}(0) F_j^{\text{brw}}(t) \rangle = 2 k_B T R_{FU} \delta(t),$$

where k_B is the Boltzmann constant, T is the temperature, $\delta(t)$ is the delta function, and R_{FU} is the resistance tensor. In contrast

to what has been done within Stokesian Dynamics [6, 24], where the resistance tensor is constant, we expect the tensor to depend on the velocity field of the fluid.

col: Short-range collision forces derived from a Yukawa potential,

$$V_{ij}^{\text{col}} \propto \frac{1}{r_{ij}} e^{-\kappa r_{ij}},$$

where κ is a system-dependent parameter and r_{ij} is the distance between the i:th and the j:th colloid ($i \neq j$).

Acknowledgements

My graduated studies at Chalmers University of Technology started in the ECMI, European Consortium for Mathematics in Industry, post-graduate program. I like to thank the local ECMI administration, Leif Arkeryd, Jöran Bergh, Peter Kumlin and Axel Ruhe (presently at the Royal Institute of Technology) for admission, initial support and encouragements. I am much obliged to the financial support from: the Network in Applied Mathematics, The Swedish Foundation for Strategic Research, and IMEGO —the Institute of Microelectronics in Gothenburg. I am grateful to Stig Larsson for superbly supervising me toward my licentiate degree, for his help, for teaching me and for his over all support. This project was initiated at the initiative of a number of people at IMEGO. I would like to thank Peter Björkholm, Anatol Krozer and Dag Billger for support, inspiration and motivation. Major parts of this project involves computer implementation of algorithms, in connection to this I would like to thank Anders Logg and Johan Jansson for introducing and helping me with Linux, C++, and Dolfin. I also would like to thank Jovan Pankovski and Chalmers reproservice for printing this report. Finally, I am thankful to the persistent support from Maria, my beloved.

References

[1] H. Aref, *Stochastic particle motion in laminar flows*, Phys. Fluids., **3** (1990), 1009–1015.

[2] H. Aref, *Development of the chaotic advection*, Phys. Fluids., **14** (2002), 1315–1325.

[3] J. Bey, *Tetrahedral grid refinements*, Computing, **55** (1995), 354–378.

[4] J.B. Birnbaum, R.S. Williams, *Physics and the information revolution*, Physics Today, **53** (2000), 38–42.

[5] D. Boffi, *Three-dimensional finite element methods for the Stokes problem*, SIAM J. Numer. Anal., **34** (1997), 664–670.

[6] J.F. Brady and G. Bossis, *Stokesian Dynamics*, Ann. Rev. Fluid Mech.**20** (1988) 111.

[7] J.H. Bramble, X. Zhang, *The analysis of multigrid methods*, in Handbook of Numerical Analysis, vol. 7, P.G. Ciarlet, J.L. Lions, eds., Elsevier (2000).

[8] S.C. Brenner, L.R. Scott, *The Mathematical Theory of Finite Element Methodes*, Springer (2002).

[9] F. Brezzi, M. Fortin, *Mixed and Hybrid Finite Element Methods*, Springer-Verlag (1991).

[10] J.P. Brody, P. Yager, R.E. Goldstein, R.H. Austin, *Biotechnology at low Reynolds numbers*, Biophys. J., **71** (1996), 3430–3441.

[11] M.A. Burns, B.N. Johnson, S.N. Brahmasandra, K. Handique, J.R. Webster, M. Krishnan, T.S. Sammarco, P. Man, D. Jones, D. Heldsinger, C.H. Mastrangelo, D.T. Burke, *An integrated nanoliter DNA analysis device*, Science, **282** (1998), 484–487.

[12] C-H. Choi, K.J.A. Westin, K. Breuer, *Apparent slip in hydrophilic and hydrophobic microchannels*, Phys. Fluids., **15** (2003), 2897–2902.

[13] A.J. Chorin, J.E. Marsden, *A Mathematical Introduction to Fluid Mechanics*, Springer (2000).

[14] M. Cieplak, J. Koplik, J.R. Banavar, *Boundary conditions at a fluid-solid interface*, Phys. Rev. Lett., **86**, 5, (2001), 803–806.

[15] C. Cercignani, *The Boltzmann Equation and its Applications*, Springer-Verlag (1988).

[16] P.M. Chaikin, T.C. Lubensky *Principles of Condense Matter Physics*, Cambridge University Press (1995).

[17] R.L. Devaney, *An Introduction to Chaotic Dynamical Systems*, Addison-Wesley (1989).

[18] L. Dieci, E.S. van Vleck, *Lyapunov spectral intervals: theory and computation*, SIAM J. Numer. Anal., **40** (2002), 516–542.

[19] R.G. Duran, R.H. Nochetto, *Weighted inf-sup and pointwise error estimates for the Stokes equations*, Math. Comp., **54** (1990), 63–79.

[20] A. Edström, *Snabbare multifysik*, Elektroniktidningen, **18** (2003), 20.

[21] H.C. Elman, *Preconditioners for saddle point problems arising in computational fluid dynamics*, Appl. Numer. Math., **43** (2002), 75–89.

[22] P.D.I. Fletcher, S.J. Haswell, E. Pombo-Villar, B.H. Warrington, P. Watts, S.Y.F. Wong, X. Zhang, *Micro reactors: principles and applications in organic synthesis*, Tetrahedron, :), **58** (2002), 4735–4757.

[23] M. Fortin, R. Glowinski, *Augmented Lagrangian Methods: Applications to the Numerical Solution of the Boundary-Value Problem*, North-Holland (1982).

[24] D.R. Foss and J.F. Brady, *Structure, diffusion and rheology of Brownian suspensions by Stokesian dynamics simulation*, J. Fluid Mech. **407** (2000), 167.

[25] V. Girault, P-A. Raviart, *Finite Element Methods for Navier-Stokes Equations*, Springer-Verlag (1986).

[26] N. Giordano, J.T. Cheng, *Microfluid mechanics: progress and opportunities*, J. Phys.: Condens. Matter., **13** (2001), R271–R295.

[27] R. Glowinski, T.W. Pan, T.I. Hesla, D.D. Joseph, and J. Périaux, *A fictitious domain approach to the direct numerical simulation of incompressible viscous flow past moving rigid bodies: application to particulate flow*, J. Comput. Phys., **169** (2001), 363–426.

[28] G.H. Golub, C. Greif, *On solving block-structured indefinite linear systems*, SIAM J. Sci. Comput., **24** (2003), 2076–2092.

[29] A. Groisman, V. Steinberg, *Elastic turbulence in a polymer solution flow*, Nature, **405** (2000), 53–55.

[30] A. Groisman, V. Steinberg, *Efficient mixing at low Reynolds number using polymer additives*, Nature, **410** (2001), 905–908.

[31] A. Groisman, M. Enzelberger, S.R. Quake , *Micofluidic memory and control devices*, Science, **300** (2003), 955–958.

[32] D.J. Harrison, K. Fluri, K. Seiler, Z. Fan, C.S. Effenhauser, A. Manz, *Micromachinig a minaturized capillary electrophoresis-based chemical analysis system on a chip*, Science, **261** (1993), 895–897.

[33] S.J. Haswell, P. Watts, *Green chemistry: synthesis in micro reactors*, Green Chemistry, **5** (2003), 240–249.

[34] J. Hoffman, A. Logg, *Dynamic Object oriented Library for Finite element computation*, `www.phi.chalmers.se/dolfin/`.

[35] H.H. Hu, N.A. Patankar, and M.Y. Zhu, *Direct numerical simulations of fluid-solid systems using the arbitrary Lagrangian-Eulerian technique*, J. Comput. Phys., **169** (2001), 427–462.

[36] I.C.F. Ipsen, *A note on preconditioning nonsymmetric matrices*, SIAM J. Sci. Comput., **23** (2001), 1050–1051.

[37] R.F. Ismagilov, A.D. Stroock, P.J.A. Kenis, G. Whitesides, *Experimental and theoretical scaling laws for transverse diffusive broadening in two-phase laminar flows in microchannels*, Appl. Phys. Lett., **76** (2000), 2376–2378.

[38] D.J. Jeffrey, *The calculation of the low Reynolds number resistance functions for two unequal spheres*, Phys. Fluids A **4** (1992), 16.

[39] D.J. Jeffrey and Y. Onishi, *Calculation of the resistance and mobility functions for two unequal rigid spheres in low-Reynolds-number flow*, J. Fluid Mech. **139** (1984), 261.

[40] A.E.Kamholz, P. Yager, *Theoretical analysis of molecular diffusion in pressure-driven laminar flow in microfluidic channels*, Biophys. J., **80** (2001), 155–160.
[41] G. Karniadakis, A. Beskok, *Micro Flow: Fundamentals and Simulations*, Springer (2002).
[42] D. Kay, D. Loghin, A. Wathen, *A preconditioner for the steady-state Navier-Stokes equations*, SIAM J. Sci. Comput., **24** (2002), 237–256.
[43] J.B. Knight, A. Vishwanath, J.P. Brody, R.H. Austin, *Hydrodynamic focusing on a silicon chip: mixing nanoliters in microseconds*, Phys. Rev. Lett., **80** (1998), 3863–3866.
[44] A.J.C Ladd, *Sedimentation of homogenous suspensions of non-Browninan spheres*, Phys. Fluids **9** (1997), 491–499.
[45] L.D. Landau, E.M. Lifshitz, *Fluid Mechanics*, Course in Theoretical Physics, vol. 6, Butterworth-Heinemann (2000).
[46] R.H Liu, M.A. Stemler, K.V. Sharp, M.G. Olsen, J.G. Santiago, R.J. Adrian, H. Aref, D.J. Beebe, *Passive mixing in a three-dimensional serpentine michrochannel*, J. Michroelectromech. Syst., **9** (2000), 190–196.
[47] L. Löfdahl, M. Gad-el-Hak, *MEMS applications in turbulence and flow control*, Prog. Aeros. Sci., **35** (1999), 101–203.
[48] A. Logg, *The multi-adaptive ODE solver*, `www.phi.chalmers.se/tanganyika/`.
[49] M. Marion, R. Temam, *Navier-Stokes Equations: Theory and Applications*, in Handbook of Numerical Analysis, vol. 6, P.G. Ciarlet, J.L. Lions, eds., Elsevier (1998).
[50] G.M. Moore, *Cramming more components onto integrated circuits*, Electronics **38** (1965).
[51] M. Mosler, U. Landman, *Formation, stability and breakup of nanojets*, Science, **289** (2000), 1165–1169.
[52] M.F. Murphy, G.H. Golub, A.J. Wathen, *A note on preconditioning for indefinite linear systems*, SIAM J. Sci. Comput., **21** (2000), 1969–1972.
[53] R. Rannacher, *Finite element methods for the incompressible Navier-Stokes equations*, in Fundamental Directions in Mathematical Fluid Mechanics, G.P. Galdi, J.G. Heywood, R. Rannacher, eds., Birkäuser Verlag, (2000).
[54] J.M. Ottino, *The Kinematics of Mixing: Streching, Chaos and Transport*, Cambrige University Press (1989).
[55] J. Pfahler, J. Harley, H. Bau *Liquid transport in micro and submicron channels*, Sensors and Actuators, A21–A23 (1990), 431–434.
[56] *Symposium on fluid mechanics of stirring and mixing*, Phys. Fluids, **3**, 5(2), (1991).
[57] Y. Saad, *A flexible inner-outer preconditioned GMRES algorithm*, SIAM J. Sci. Comput., **14** (1993), 461-469.
[58] Y. Saad, *Iterative Methods for Sparse Linear Systems*, SIAM (2003).
[59] R.F. Service, *Comming soon: the pocket DNA sequencer*, Science, **282** (1998), 399–401, and *Miniaturization puts chemical plants where you want them*, Science, **282** (1998), 400.
[60] V. Simoncini, D.B. Szyld, *Flexible inner-outer Krylov subspace methods*, SIAM J. Numer. Anal., **40** (2003), 2219–2239.

[61] A.D. Stroock, S.K.W. Dertinger, A. Ajdari, G.M. Whitesides, *Chaotic mixer for microchannels*, Science, **295** (2002), 647–651.

[62] P. Styring, *Microfluidics: History, Theory and Application*, Advanced course at the International Centre for Mechanical Sciences, Udine, Italy, private comunication (2003).

[63] H. Song, M.R. Bringer, J.D. Tice, C.J. Gerdts, R.F. Ismagilov, *Experimental test of scaling of mixing by chaotic advection in droplets moving through microfluidic channels*, Appl. Phys. Lett., (in press), (2003).

[64] *The millennium prize problems*, Clay Mathematic Institute, `www.claymath.org`.

[65] P.A. Thompson, S.M. Troian, *A general boundary condition for liquid flow at solid surfaces*, Nature, **389** (1997), 360–362.

[66] T. Thorsen, S.J. Maerkl, S.R. Quake, *Microfluidic large-scale integration*, Science, **298** (2002), 580–584.

[67] G. Tryggvason, B. Bunner, A. Esmaeeli, D. Juric, N. Al-Rawahi, W. Tauber, J. Han, S. Nas and Y.-J. Jan, *A front-tracking method for the computatios of multiphase flow*, J. Comput. Phys., **169** (2001), 708–759.

[68] S. Turek, *Efficient Solvers for Incompressible Flow Problems: An Algoritmic and Computaional Approach*, vol. 6 in Lecture Notes in Computational Science and Engineering, Springer (1999).

[69] J. Volker, L. Tobiska, *Numerical performance of smoothers in coupled multigrid methodes for the parallel solution of the incompressible Navier-Stokes equations*, Int. J. Numer. Meth. Fuids, **33** (2000), 453–473.

[70] J. Volker, G. Matthies, *Higher-order finite element discretizations in benchmark problems for incompressible flows*, Int. J. Numer. Meth. Fuids, **37** (2001), 885–903.

[71] J. Volker, *Higher order finite element methodes and multigrid solvers in a benchmark problem for 3D Navier-Stokes equations*, Int. J. Numer. Meth. Fuids, **40** (2002), 775–798.

[72] B.H. Weigl, P. Yager, *Microfluidic diffusion-based separation and detection*, Science, **283** (1999), 346–347.

[73] P. Wesseling, C.W. Oosterlee, *Geometric multigrid with applications to computational fluid dynamics*, J. Comput. Appl. Math., **128** (2001), 311–334.

[74] G.M. Whitesides, A.D Stroock, *Flexible methods for microfluidics*, Physics Today, **54** (2001), 42–48.

[75] Y. Zhu, S. Granick, *Limits of hydrodynamic non-slip boundary condition*, Phys. Rev. Lett., **88** (2002), 1–4.